Quantitative Energy Storage and Ejection Release in Superelastic Shape Memory Alloy Wire

Wen-Chao Sui[1], Yong-Chen Pei[1,*], Bao-Hua Wang[1], Ji-Tuo Wu[1], Huiqi Lu[2]

[1]School of Mechanical and Aerospace Engineering, Jilin University, Nanling Campus, Changchun, 130025, People's Republic of China

[2]Institute of Biomedical Engineering, Department of Engineering Science, University of Oxford, Oxford, OX3 7DQ, United Kingdom

Abstract: Superelastic shape memory alloy (SMA) wire is a memorable deformation material with large resilience and high energy density. In this paper, a revolutionary and yet explainable property of the SMA is investigated and confirmed: superelastic SMA energy storage and release can be quantitatively measured using electrical resistance. This finding boosted the SMA with significant advantages and potential in the field of mechanical energy storage and ejection release. In this project, a state-of-the-art energy storage ejection device is designed to test the relationship among SMA wires' stress, strain, and resistance change rate. The electrical resistance, ejection energy density and energy conversion efficiency are studied in the SMA wire energy tests. The experimental results confirm that the resistance change rate of the superelastic SMA wire has a stable linear relationship with the strain. The ejection energy density increases with the resistance change rate. A theoretical model of the relationship between the ejection energy density and resistance change rate is established based on the experimental results. In conclusion, coupled with its shape memory property, the superelastic SMA can achieve sophisticated tasks that require 'programmable' and predictable energy storage or ejection.

Keywords: shape memory alloy wire, quantitative measurement, superelasticity, shape memory effect, energy storage, energy ejection.

*Corresponding author.

E-mail address: peiyc@jlu.edu.cn (Y.-C. Pei).

1. Introduction

Shape memory alloy (SMA) are well known for its superelasticity and shape memory effect [1]. SMA's superelasticity property refers to its ability to undergo extensive revertible deformations [6]. SMA in the austenite state induces martensite transformation under the action of an external force, which results in deformation and recovery after the stress is removed [1]. SMA's shape memory effects can be triggered by different triggering methods, such as magnetic triggering and thermal triggering [2-4]. One of the most commonly used SMAs is nickel-titanium (NiTi) SMA. Its shape memory effect can be triggered by thermal effects.

SMA wires play a unique and significant role in the field of smart materials and are widely used in structural engineering, biomedical, aerospace and other fields [8-13]. The superelastic NiTi SMA wire is a cost-effective material with an enormous strain but a small driving force [8]. It is preferable for industrial applications due to its stability and practicability compared to the cheaper copper-based alternatives. Compared with spring steel, the strain and energy density of superelastic NiTi SMA wire are six times more than those of spring steel [14]. There is a new material called nanocomposites. Shijie Hao et al. prepared nanocomposites with excellent mechanical properties, and the mechanical energy storage efficiency and energy density were significantly improved [14]. However, the nanocomposites are still in the experimental stage and are not yet ready for industrial deployment or commercial applications. Compared with NiTi SMA, nanocomposites require large driving stress

and higher cost.

For decades, researchers have conducted and are still conducting investigations on the properties of SMA. Many applications are developed based on the shape memory effect and the superelasticity of SMA. For example, the shape memory effect of SMA can be used in actuators. Junfeng Li proposed a control method based on bending force prediction to improve the position tracking accuracy of SMA soft robots [5]. The superelasticity of SMA has been used to determine the stress and strain state by measuring the resistance of the SMA wire [7].

The stress-strain relationship of superelastic SMA wire has the characteristics of hysteresis and a specific hysteresis area. Therefore, there are more studies on damping characteristics but fewer studies on energy storage and ejection release [15]. Seong-Cheol Kwon et al. used SMA superelasticity to improve the performance of traditional spring-blade gears and verified the effectiveness of SMA gears in isolating micro-jitter [16]. Samir B. Kumbhar et al. changed the modulus of SMA wire by a DC power supply and studied the dynamic response of the system when SMA was combined with a magnetorheological elastomer as a smart spring-mass damping system in a tuned shock absorber [17].

There are limitations in previous studies. Schmidt et al. studied the damping capacity of superelastic NiTi SMA wire, but ignored the energy storage capacity and the ejection energy release capacity [18]. E. Pieczyska et al. found that the recoverable strain energy of SMA increases and the dissipation energy decreases at high strain rates, but the relationship between strain, electrical resistance and energy

density was not defined [19].

Other main advantages of using the superelastic NiTi SMA wires are that it has good fatigue resistance and large recoverable strain. Previous studies have shown that the resistance change rate of superelastic NiTi SMA wire has a good linear relationship with strain, and its mechanical properties are stable [20, 21]. Zhiqiang Liu et al. studied the resistance–stress-strain relationship of SMA and found a linear relationship between the resistance change rate and strain [20]. In addition,

The process of instantaneous release of stored energy is called energy storage ejection. Mechanical energy storage ejection is a launch method with an indispensable position in military applications. This technology has been used for weapon launches, including gunpowder launches, pneumatic ejection, electromagnetic ejection and many other forms. [ref] However, designing and manufacturing a safe and stable energy storage launcher remains a huge challenge. Existing materials cannot store energy quantitatively or release the energy in a ‘programmable’ manner. In comparison, superelastic SMA is an advanced material for energy storage and release.

Mechanical energy storage and equipment simplification play a vital role in energy technology research. SMA has a large elastic energy storage capacity. The recoverable conversion strain of SMA wire can reach 8% [23]. In previous studies, there were only a handful of studies on mechanical energy storage measurement and energy release monitoring. Ondrej Rubes et al. proposed an electromagnetic energy harvesting device that converts the kinetic energy of environmental mechanical vibrations using electrical signals from piezoelectric patches to monitor mechanical

vibrations [22]. This study demonstrated that SMA wire energy storage launch technology is a novel and meaningful method in designing energy storage and ejection devices. Moreover, using SMA wire energy storage catapults can significantly reduce the size and the weight of the launcher with a reduced cost. More importantly, the amount of ejection energy can be precisely controlled, which is of great value in the launch field.

This paper focuses on studying and confirming the quantitative energy storage and ejection release of superelastic SMA wires. Firstly, a test device was designed and used for studying tensioned superelastic NiTi SMA wires. Secondly, the quantitative energy storage and energy ejection were studied and reported using different superelastic NiTi SMA wires. After testing NiTi SMA wires with different diameters, lengths and loading forces and studying the mechanical behaviour of the energy storage ejection, the energy storage ejection law of superelastic SMA wire is defined. Moreover, indicators such as resistance change rate, stress, strain and energy conversion efficiency are also tested and confirmed. Finally, a theoretical and mathematical model was developed to define the relationship between the ejection energy density and the resistance change.

2. Experiment designs and SMA Wire settings

2.1 SMA Wire Test Device

An in-house state-of-the-art test device was designed and built to test the energy

storage and ejection of the superelastic SMA wire. This device can control the loading time, loading force and displacement, and record electrical resistance and ejection velocity. The block diagram of the design of this test device is shown in Fig. 1.

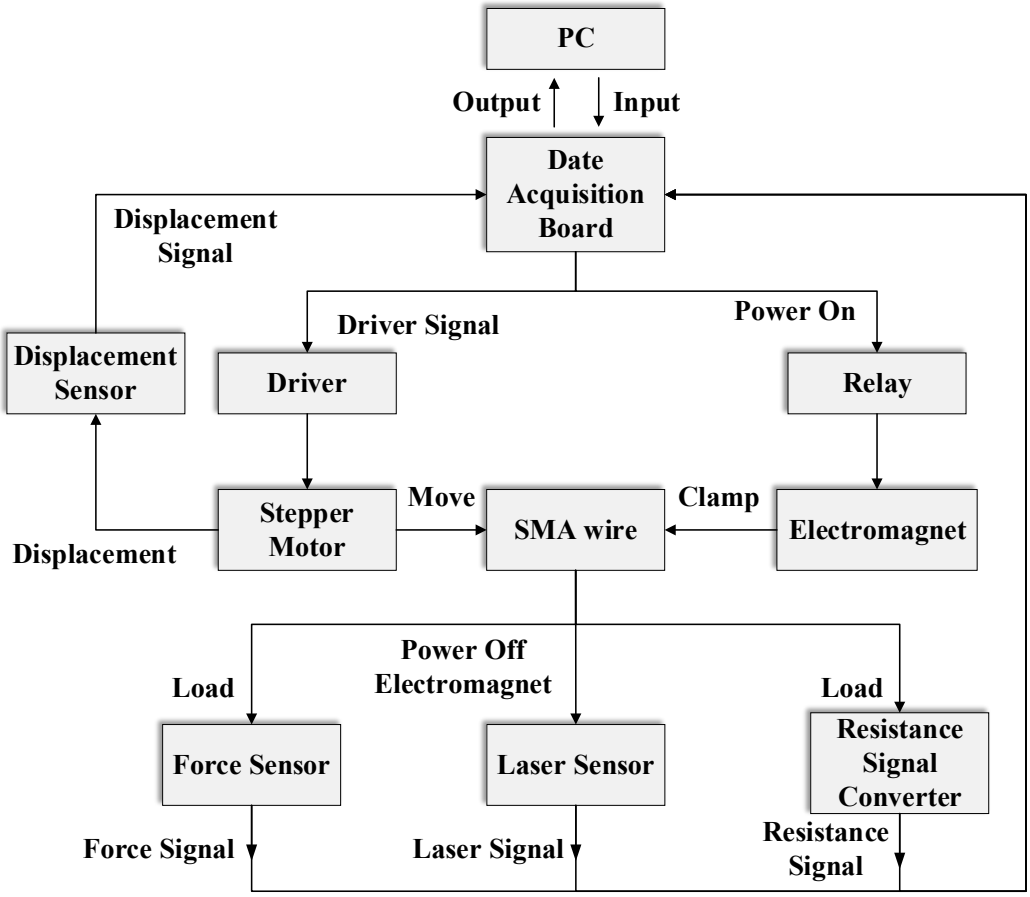
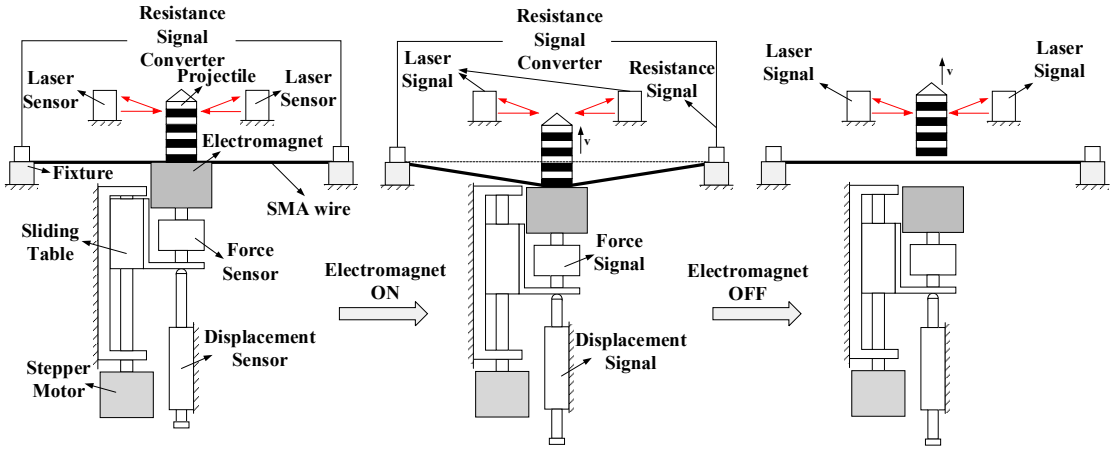


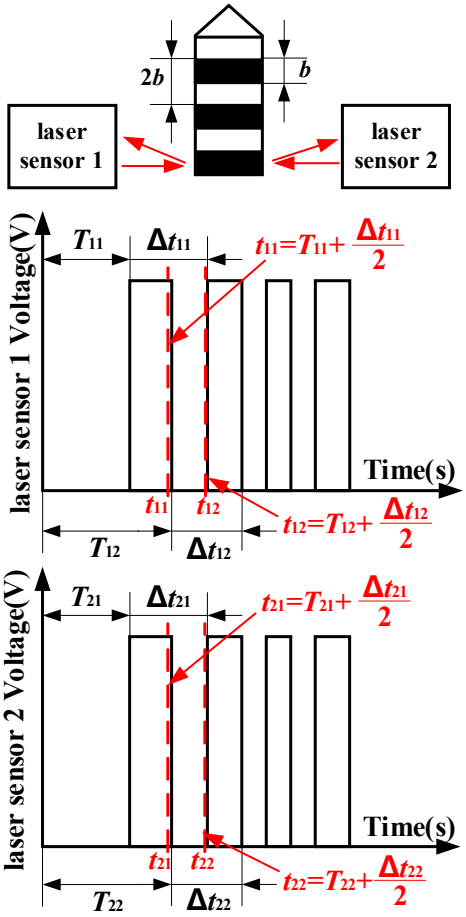
Fig. 1. Block diagram of the design of the wire test platform.

In this test platform, a computer workstation is used as a control unit to control the loading time of the test equipment by turning the electromagnet on and off. [move the specification of the workstation to here]. As shown in Fig. 1, the data acquisition board acts as an intermediate bridge by transmitting the commands from the workstation to the stepper motor driver and relay. Collected signals from the force sensor, laser sensor and rethe resistance signals will be returned to data acquisition board before transmitting to the computer workstation of signal processing and analysis.

Detials of the test processes of energy ejection and velocity signal conversion are shown in Fig. 2. The superelastic SMA wire is clamped between the projectile and the electromagnet. The stepping motor loads the superelastic SMA wire by driving the sliding table to move down. When the set loading time is reached, the electromagnet will be turned powered off, the projectile will eject upwards, and the laser sensor will detect the projectile velocity simultaneously.



(a)



(b)

Fig. 2. Test Device Diagram. (a) Ejection test process. (b) Signal and velocity conversion.

As shown in Fig. 2(a) and Fig. 3, the superelastic SMA wire is clamped at both ends by clamps that composed of clamping bolts and bakelite. Each clamping bolt has a radial through hole. SMA wire passes through both holes. The bakelite is connected to a U-shaped bracket. The length of the SMA wire can be adjusted by changing the position of the bakelite on the U-shaped bracket. The resistance signal line is connected to the clamping bolts at both ends. The other end of the signal wire is connected to a resistance signal converter to directly obtain the resistance signal of the SMA wire. When the electromagnet is switched on, force and resistance signals are recorded and converted to electric signals. When the electromagnetic switch is turned off, the energy stored in the SMA wire will be released. The changing magnetic field

is caused by the electromagnet being energized and de-energized. At the same time, the closed-loop circuit formed by the SMA wire and the resistance signal wire will generate current under the alternating magnetic field.

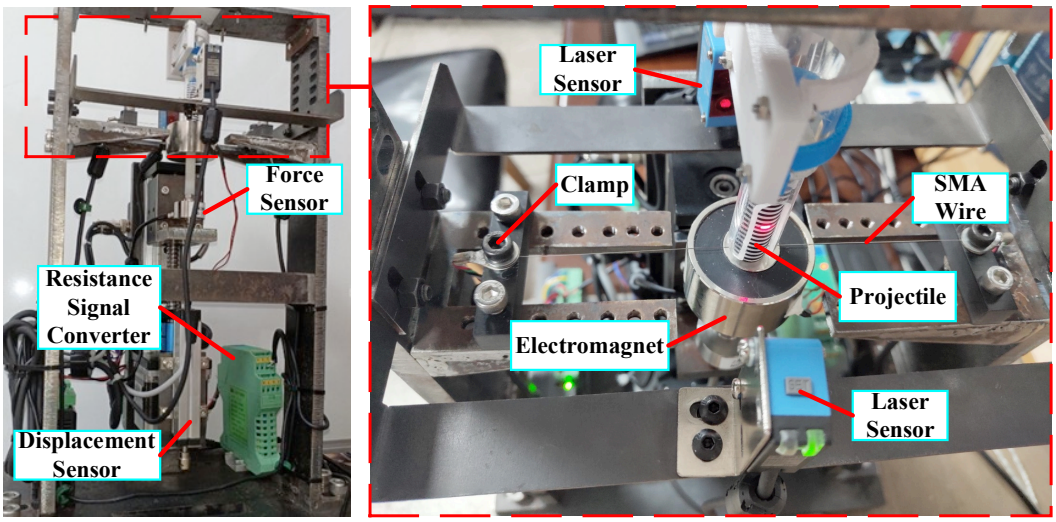


Fig. 3. Projection and side views of the test device.

When desgining this test device, one challenge is to avoid interference during resistance signals collection.. In order to reduce interference, the superelastic SMA wire need to be insulated from the test device. In this test device, the closed-loop circuit and the magnetic field generated by the electromagnet are parallel and symmetrical.

As shown in Fig. 3, the velocity test device consists of two laser sensors, a signal conversion module and a laser sensor bracket. The cylindrical surface of the projectile is pasted with strips spaced in black and white, and the unit width of the strip is b. In this experiment, b = 1 mm. When the laser is irradiated on the black stripe, it outputs a low-level signal; when the laser is irradiated on the white stripe, it outputs a high-level signal. The projectile shoots out, and the laser sensor outputs a signal level corresponding to the changing black and white stripes. To reduce the strip width error

and the sensitivity error of the laser sensor to the black and white stripes, the adjacent black and white stripes are combined into a strip with a width of 2*b*, that is, a high level and a low level of adjacent signals are combined into a signal group. By analysing multiple adjacent signal groups together, this device can accurately measure the total displacement and the time difference. The ejection velocity of the projectile (ejection velocity) is defined as the ratio of the displacement and the time difference. In this system, the maximum ejection velocity is used as the maximum velocity of the projectile ejected by the superelastic SMA wire. As shown in Fig. 2(b), the square wave signal are generated by the two laser sensors and velocity conversions.

Among them, time t_{11} is the middle time of Δt_{11}, and its velocity $v_{11} = 2b / \Delta t_{11}$; time t_{12} is the middle time of Δt_{12}, and its velocity $v_{12} = 2b / \Delta t_{12}$; time t_{21} is the middle time of Δt_{21}, and its velocity $v_{21} = 2b / \Delta t_{21}$; time t_{22} is the middle time of Δt_{22}, and its velocity $v_{22} = 2b / \Delta t_{22}$.

The parameters of four sensors that used in this test device are shown in Table 1.

Table 1. Sensor parameters.

Sensor	Resolution accuracy	Range
Displacement sensor	0.01 mm	3-50 mm
Resistance signal converter	0.06 Ω	0-30 Ω
Force sensor	0.1 N	±50 N
Laser sensor	50 μs	\

The resolution accuracy of the displacement sensor is the maximum error that the sensor can tolerate in printing errors of the black and white strips, which is 0.01 mm. When the projectile was ejected, the velocity was measured by measuring the change

in the strip with the laser sensor. The ejection velocity can be precisely measured from the ratio of the unit strip width to the response time. The printing error of the strip is divided by the response time of the laser sensor to obtain a maximum velocity error of 0.2 m/s. The test velocity of this paper can reach 4-5 m/s, thereby the accuracy of this can be guaranteed.

2.2 Shape Memory Alloy Wire and Wire Pretreatment

The energy tests of superelastic NiTi SMA wires were underatnken in room temperature (20±2°C). The chemical composition of NiTi SMA includes 43.76% Ti, 56.2% Ni, O ≤ 0.05%, H ≤ 0.005%, and C ≤ 0.07%. The selected superelastic SMA wire includes three wire diameters of 0.1 mm, 0.15 mm, and 0.2 mm.

Frislty, repeated tensile tests on superelastic SMA wire were carried out before the test. This pre-test is to ensure that the test results are solid and repeatable. By increasing a certain residual strain, a stable stress–strain curve can be obtained. The pretreatment process is as follows: Superelastic SMA wires of different wire diameters are cut into a length of approximately 190 mm to ensure the effective length, as shown in Fig. 4. Under different wire diameter conditions, the stress at the end of superelastic deformation is different, and the maximum deformation is 6% to 8%. The pretreatment adopts the cyclic method of equal strain. The strain amount is 7%, and the cyclic stretching is 20 times. Superelastic SMA wires of different wire diameters are trained.

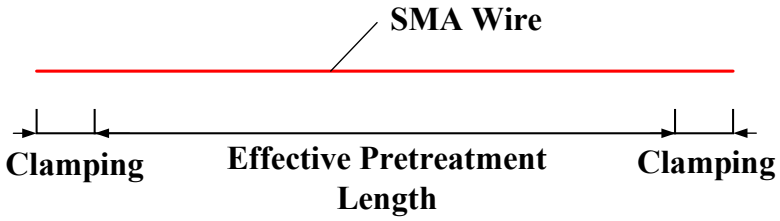
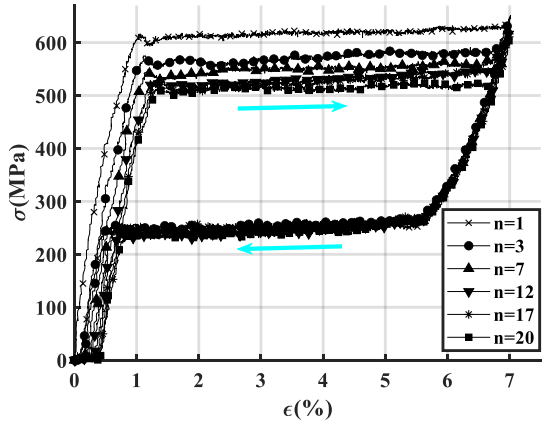


Fig. 4. Effective length of the superelastic SMA wire during pretreatment.

As shown in Fig. 5, after multiple tensile tests, the total residual strain gradually stabilized, the hysteresis curve became stable, and the repeatability was greatly improved. It has been observed that the phase transformation stress changes significantly during loading and the stress plateau moves down significantly. With the increase in the number of cycles, the stress of martensitic transformation for 0.1 mm and 0.2 mm SMA wires is reduced from 600 MPa to approximately 500 MPa, and the stress for the transformation for SMA wires of 0.15 mm is reduced from 530 MPa to approximately 400 MPa. When unloading, the stress remains steady during the reverse transformation from martensite to austenite. The stresses of the 0.1 mm, 0.15 mm and 0.2 mm SMA wires were maintained at approximately 250 MPa, 200 MPa, and 300 MPa, respectively.



(a)

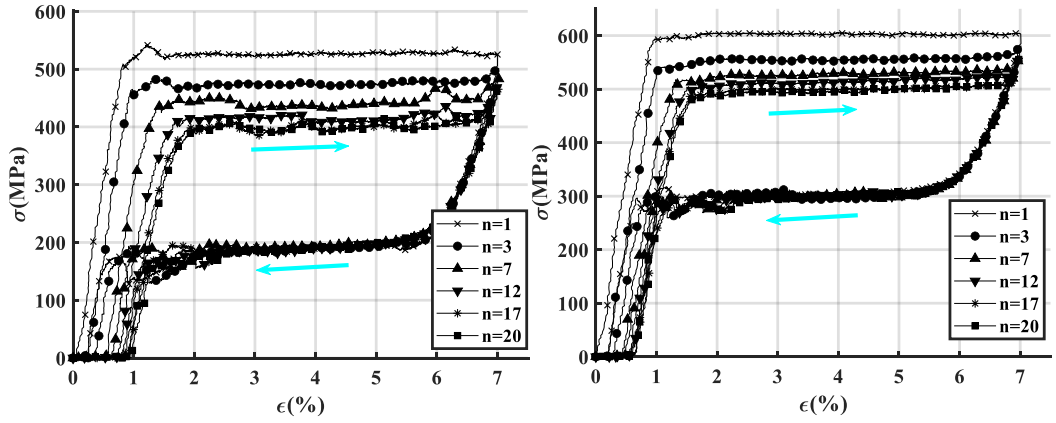


Fig. 5. Stress and strain during pretreatment of Superelastic SMA wire. (a) d = 0.1 mm. (b) d = 0.15 mm. (c) d = 0.2 mm.

2.3 Test Method and Process

In this test, superelastic SMA wires with different diameters and lengths were used as the experimental group. To compare the quantative energy storage characteristics between superelastic SMA and steel wires, steels with wire diameters of 0.1 mm and 0.2 mm (0.15 was not available) were used as the control group. The test parameters and conditions for SMA and steel wires are reported in Table 2.

Table 2. Experimental and control groups with different wire diameters.

Wire diameter/mm	SMA wire experimental group/mm			Steel wire control group/mm		
0.1	100	120	140	100	120	140
0.15	100	120	140	/	/	/
0.2	100	120	140	100	120	140

For both the experimental and control groups, multiple consecutive energy storage

ejection tests were carried out in a gradual loading mode. In these tests, each test has a larger load than the previous test. According to the previous test results, the positions where the resistance change rate of different test groups is 10%, 20%, and 30% are determined. The test in each position will be repeated in 20 groups. The test data of all test groups will be collected and analysed.

During this experiment, the maximum loading stroke is controlled to minimize the risk of superelastic SMA wire breaking. The strain of the SMA wire is controlled within 7% during the test, calculated based on the stress–strain curve during pretreatment (Fig. 5).

3. Energy storage and ejection release

The experiments of superelastic SMA wires are mainly divided into the loading energy storage stage and the ejection release stage. This section explains the theoretical calculation method of energy density and efficiency.

In the loading energy storage stage, the SMA wire is loaded from the initial length to the designated length. In the ejection release stage, the SMA wire is instantly restored from the designated length to the initial length and the projectile eject upwards using the energies released from the wire. The SMA wire will return to its initial length when its internal stored energy are completely released.

According to the loading method of the test device, the force analysis of the superelastic SMA wire is modelled and demonstrated in Fig. 6.

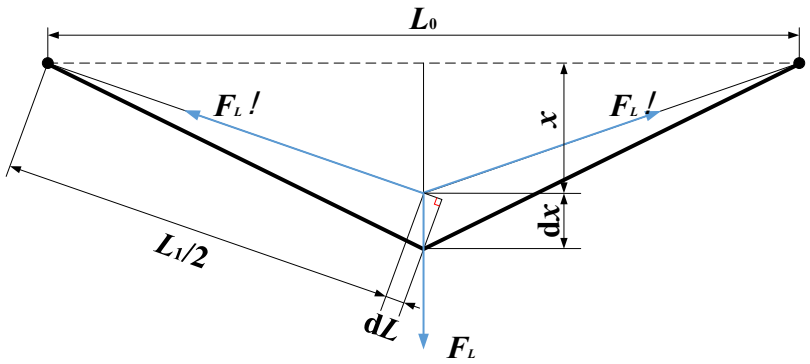


Fig. 6. Force analysis of SMA wire.

In the test, the cumulative forces loaded by the test bench are defined as W_L

$$W_L = \int F_L \mathrm{d}x \tag{1}$$

where F_L is the loading force of the test bench, F_L increases with increasing displacement, and dx is the slight displacement along the loading direction when the SMA wire is loaded.

The cumulative force of the component forces on the SMA wire is defined as W_L'

$$W_L' = \int 2F_L' \mathrm{d}L \tag{2}$$

where F_L' is the axial force of the SMA wire and dL is half of the differential amount of SMA wire.

According to Fig. 6 and the trigonometric function equation, it can be calculated

$$\frac{L_1}{2} = \sqrt{(\frac{L_0}{2})^2 + x^2} \tag{3}$$

$$\frac{x}{(\frac{L_1}{2})} = \frac{\mathrm{d}L}{\mathrm{d}x} \tag{4}$$

$$\frac{x}{\sqrt{(\frac{L_0}{2})^2 + x^2}} = \frac{F}{2F_1} \tag{5}$$

where L_0 is the original length of the superelastic SMA wire, L_1 is the length of the SMA wire before the change, and x is the displacement of the SMA wire before the

change.

Equations 1-5 can be converted into

$$W_L' = \int 2F_L' \mathrm{d}L = \int F_L \mathrm{d}x = W_L \tag{6}$$

According to equation 6, the cumulative forces loaded by the test bench can be directly calculated by equation 1 without conversion. This simplifies the calculation of energy during loading.

In the process of energy storage and release of superelastic SMA wire, in addition to the elastic energy stored and released, a part of the energy will be lost. The forms of energy loss in this test are summarized as follows: damping and phase change loss of superelastic SMA wire; friction loss between the projectile and the duct wall when the projectile is released; the projectile and electromagnet have a small amount of magnetic force that causes energy loss after the electromagnet is powered off; and other forms of energy losses, e.g., sound energy released during loading and unloading of superelastic SMA wire.

The energy stored by the superelastic SMA wire, which is the cumulative force loaded by the test bench, W_L

$$W_L = W_A + W_C \tag{7}$$

where W_A is the work done on the projectile and W_C is the energy lost when the superelastic SMA wire releases the projectile. When the energy of the SMA wire is completely released, the stored energy is mainly converted into the kinetic energy and the gravitational potential energy of the projectile.

Total energy obtained by the projectile, W_A

$$W_A = \frac{1}{2}mv^2 + mgh \tag{8}$$

where m is the mass of the projectile; v is the maximum velocity when the projectile is released; g is the gravitational acceleration, 9.8 m/s; and h is the height difference between the projectile before it is released and the initial position.

The energy density measurement index is adopted to describe the relationship between the energy storage and energy release of the superelastic SMA wire. Energy density is divided into volume energy density and mass energy density. The energy stored per unit volume is called the volume energy density, and the energy stored per unit mass is called the mass energy density. This paper uses volume energy density, and this study only considers the ejection energy density D_{WV}

$$D_{WV} = \frac{W_A}{V} \tag{9}$$

where V is the volume of the superelastic SMA wire.

According to E.M. Sharifi and V. Apostol's research [24, 25], energy conversion efficiency refers to the ratio of the work done by the SMA wire to the energy stored. The energy conversion efficiency η

$$\eta = \frac{W_A}{W_L} \tag{10}$$

4. Results and Discussion

To obtain the complete ejection velocity, the ejection height of the projectile is

higher than the laser position. Therefore, each ejection test should ensure enough ejection energy, which can obtain the minimum load position through the pretest.

4.1 Stress–Strain Relationship

In this experiment, the superelastic SMA wire is subjected to a radial loading force. The relationship between the radial loading force and displacement can be divided into three stages. In the initial loading stage, the loading force is almost unchanged as the displacement increases. In the mid-term loading stage, the loading force in this stage rises at a uniform velocity with increasing displacement. In the later loading stage, the loading force rises rapidly with increasing displacement.

The axial stress σ of the SMA wire

$$\sigma=\frac{F_L'}{\pi(\frac{d}{2})^2} \tag{11}$$

where d is the diameter of the SMA wire. In this study, there are three types of d: 0.1 mm, 0.15 mm, and 0.2 mm.

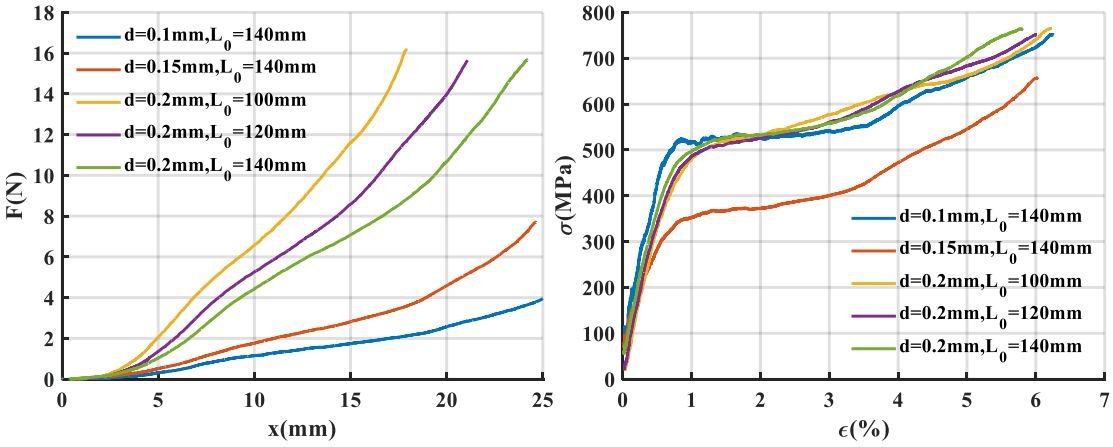
The strain of SMA wire, ε

$$\varepsilon=\frac{2\Delta L}{L_0} \tag{12}$$

where ΔL is the total deformation of the SMA wire after loading.

The force-displacement relationship is shown in Fig. 7(a). Fig. 7(a) is transformed by equations 3-5, 11, and 12 to obtain the stress–strain relationship. Fig. 7(b) shows that before the strain of the SMA wire reaches 0.8%, the stress rises sharply with increasing strain. At this moment, it is in the stage of austenite elastic deformation. A

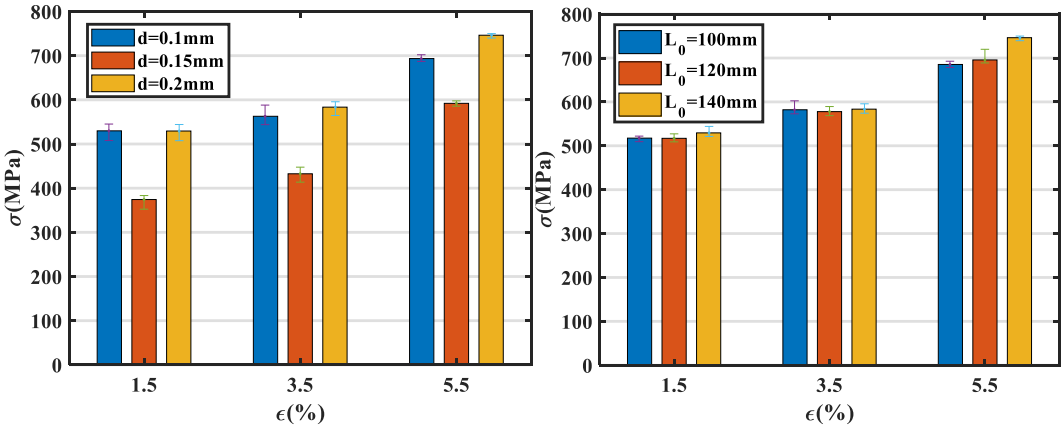
turning point occurs when the strain reaches approximately 0.8%, and a stress yield plateau appears when the strain reaches 0.8-3.2%. The rate of stress change increases when the strain is greater than 3.2%. When the strain is approximately 0.8%-6%, it can be regarded as the martensitic transformation stage. Fig. 7(b) shows that the phase transition stress of the 0.15 mm SMA wire is lower than that of the 0.1 mm and 0.2 mm wires. It should be emphasized that the 0.15 mm SMA wire comes from different batches.



(a) (b)

Fig. 7. Relevant tensile data of SMA wire. (a) Relationship between the force and displacement. (b) Relationship between the stress and strain.

Fig. 8 shows the effect of different strains on the stress of SMA wires of different diameters. As shown in Fig. 8(a), the stress of SMA wires is significantly different under the same length but with different wire diameters. Under the same wire diameter condition, comparing the stresses of SMA wires with different lengths, the stresses under the same strain state are almost equal, as shown in Fig. 8(b). This is caused by the difference in the manufacturing process of SMA wires with different wire diameters. It can be seen from the figure that the stress strain has good repeatability, and the stress regularity increases and shows consistency.

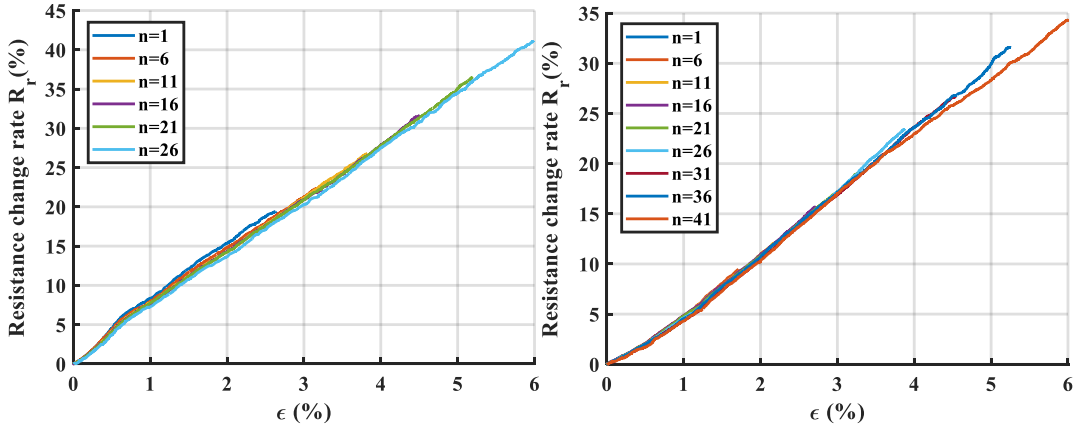


(a) (b)

Fig. 8. Comparison of stress. (a) Under different wire diameters and strain conditions, L_0 = 140 mm. (b) Under different length and strain conditions, d = 0.2 mm.

4.2 Resistance Change Rate-Strain Relationship

The resistance change rate of the superelastic SMA wire and strain have a linear relationship. Fig. 9 deomonstrates the resistance change rate R_r under different strains. As shown in Fig. 9(a)-(e), the resistance change rate increases linealry when stain increases.



(a) (b)

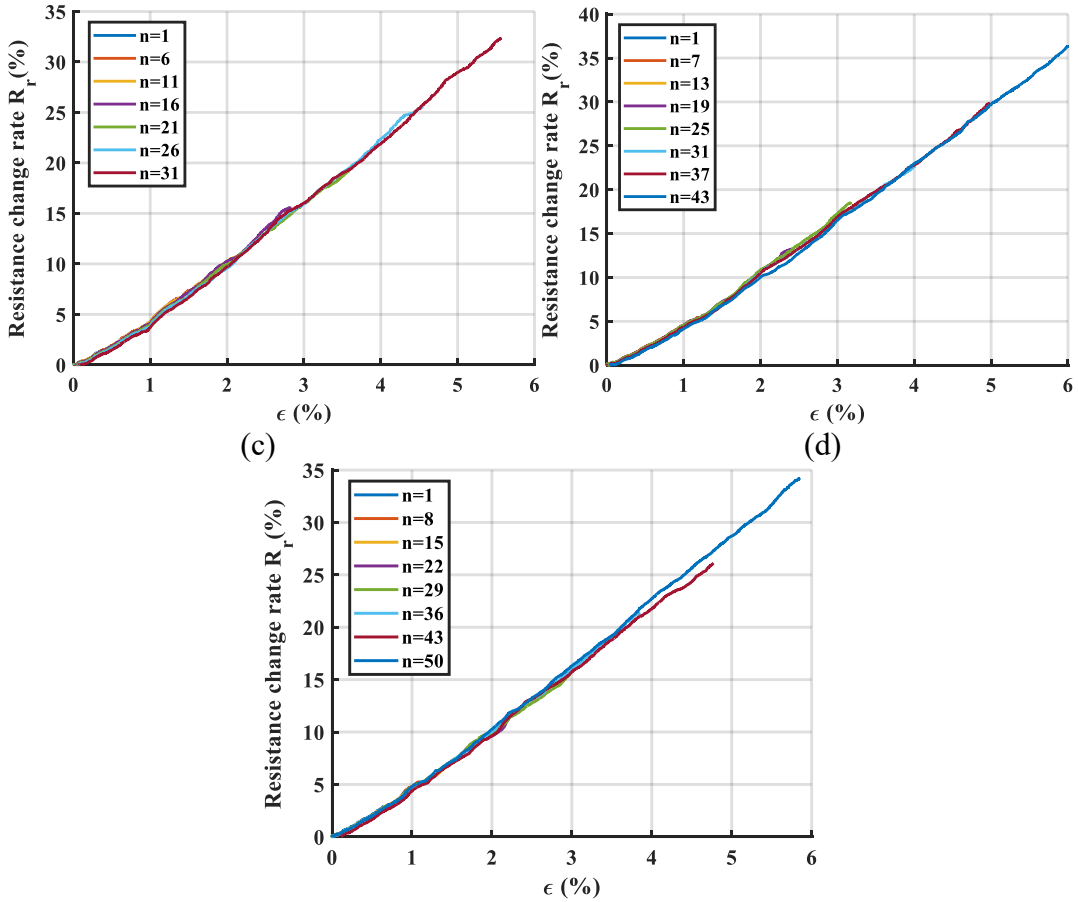
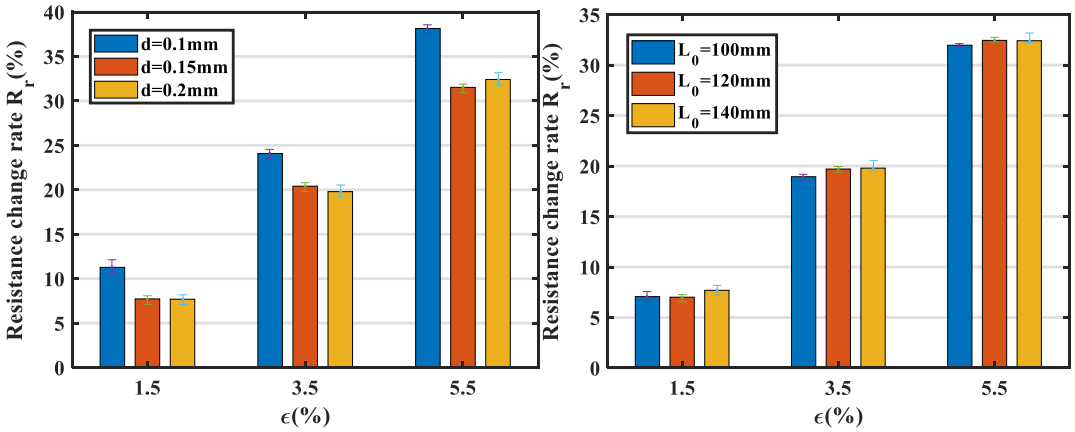


Fig. 9. Resistance change rate R_r under different strain conditions. (a) d = 0.1 mm, L_0 = 140 mm. (b) d = 0.15 mm, L_0 = 140 mm. (c) d = 0.2 mm, L_0 = 100 mm. (d) d = 0.2 mm, L_0 = 120 mm. (e) d = 0.2 mm, L_0 = 140 mm.

Fig. 10 shows the influence of the wire diameter and length on the resistance change rate under different strains. As the strain increases, the resistance change rate of the SMA wire also increases. Fig. 10(a) demonstrates that the resistance change rate of the 0.1 mm SMA wire is the largest among three groups, and the resistance rates of the 0.15 mm and 0.2 mm SMA wires are approximately the same. Fig. 10(b) shows that the resistance change rate of each strain is similar under certain wire diameter conditions. There are many factors that affect resistance, including resistivity, wire diameter and length. Moreover, the alloy phase structure of the superelastic SMA wire is constantly changing during the superelastic strain process. The resistivity of SMA wires, wire diameter and length are confounders that affect the resistance

change rate. SMA wires with different wire diameters or length have different resistance change rate.



(a) (b)

Fig. 10. Comparison of the resistance change rate R_r. (a) Under different wire diameters and strains, L_0 = 140 mm. (b) Under different lengths and strains, d = 0.2 mm.

4.3 The Relationship Between Resistance Self-Sensing and Energy

In this section, the relationship between the self-sensing resistance of superelastic SMA wire and the energy of ejection is studied. Fig. 11 shows the energy released per unit volume of the superelastic SMA wire with the increase in the resistance change rate, that is, the ejection energy density D_{WV}. Fig. 12 shows the relationship between the resistance change rate and the ejection energy density under different wire diameters and lengths. Fig. 13 shows the relationship between different resistance change rates and energy conversion efficiency.

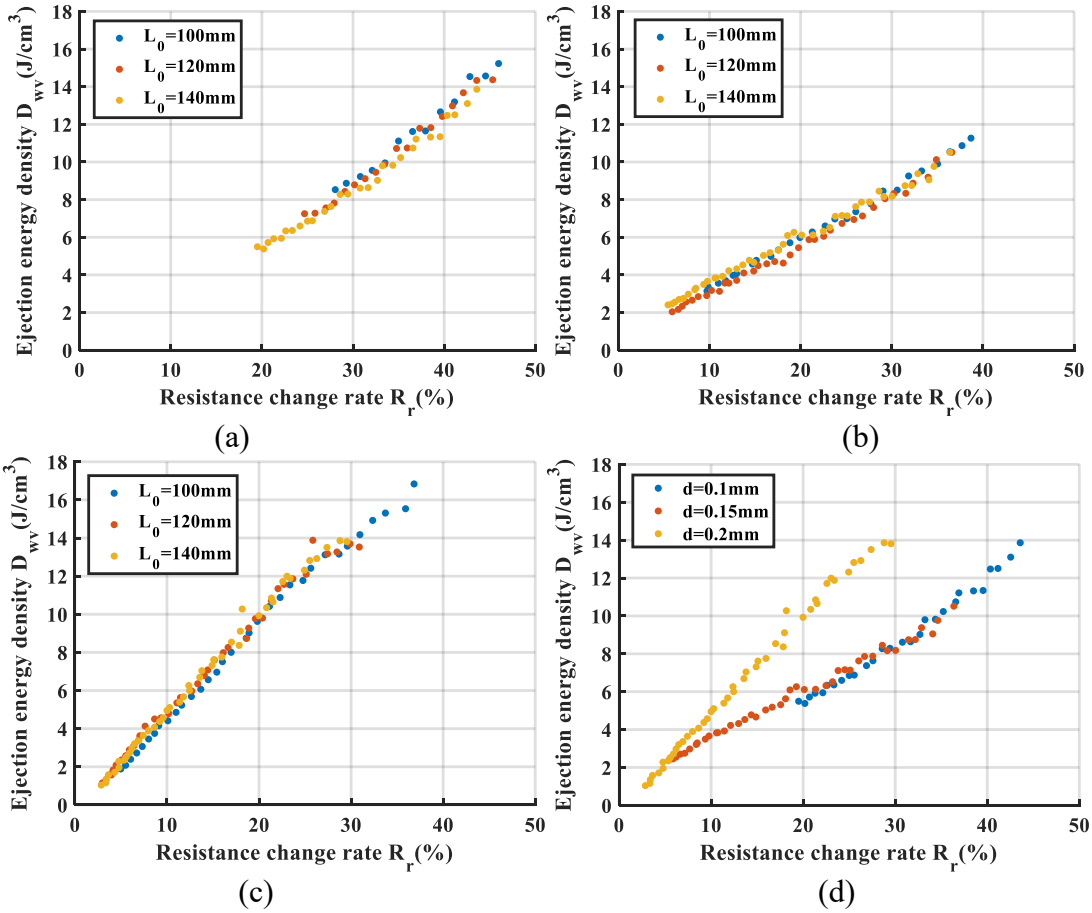


Fig. 11. Comparison of ejection energy density and resistance change rate R_r. (a) d = 0.1 mm. (b) d = 0.15 mm. (c) d = 0.2 mm. (d) L_0 = 140 mm.

As shown in Fig. 11(a)-(c), as the resistance change rate increases, which is the strain increase, the ejection energy density of the superelastic SMA wire increases linearly. Among them, under different length conditions of 0.1 mm and 0.15 mm superelastic SMA wire, there is little difference in the ejection energy density under the same resistance change rate. This is caused by the different pretightening forces of the fixed SMA wire during the test.

According to Fig. 11(d), the ejection energy density of the SMA wire with wire diameters of 0.1 mm and 0.15 mm is almost equal. However, it can still be seen that the ejection energy density growth rate of the 0.1 mm wire diameter is slightly larger than that of 0.15 mm, and the ejection energy density of the 0.2 mm SMA wire is

much larger than the energy density of 0.1 mm and 0.15 mm.

Fig. 12(a) shows that the ejection energy density of the 0.2 mm superelastic SMA wire is larger than that of 0.15 mm. In Fig. 12(b), under the same wire diameter and each resistance change rate state, the ejection energy density of the SMA wire increases only slightly when the length of the SMA wire increases. This result corresponds to the energy density under the hysteresis curve of the preconditioning, which is the area under the stress–strain curve when the tension is released.

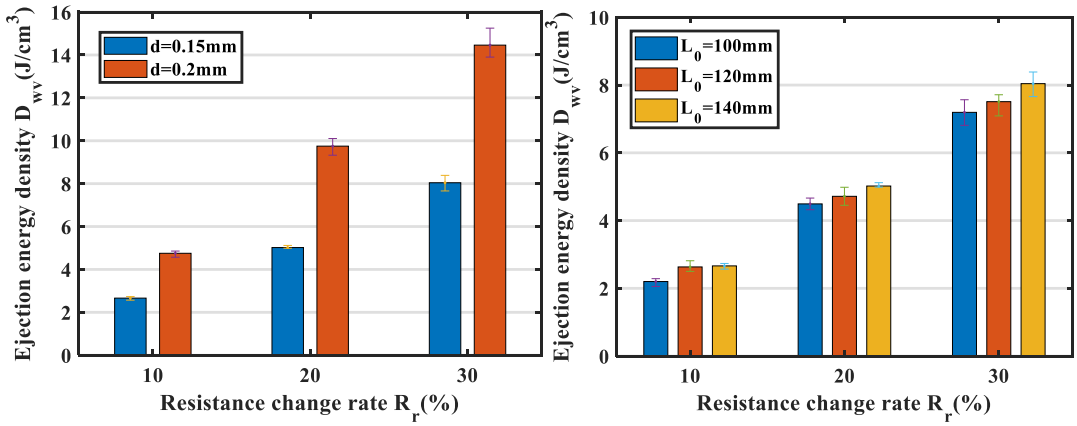


Fig. 12. Comparison of ejection energy density. (a) Under different wire diameters and resistance change rates R_r, L_0 = 140 mm. (b) Under different lengths and resistance change rates R_r, d = 0.15 mm.

As shown in Fig. 13, at the same wire diameter, the energy conversion efficiency of superelastic SMA wires of different lengths is similar. As the resistance change rate increases, the energy conversion efficiency shows a downwards trend. Fig. 13(a) shows that the energy conversion efficiency of the 0.1 mm SMA wire is approximately 40%, the efficiency of the 0.15 mm SMA wire is 40 - 60%, and the efficiency of the 0.2 mm SMA wire is the highest, which can reach more than 60%. In conjunction with Fig. 5, it can be seen that the energy conversion efficiency during ejection is affected by the phase change platform during loading and unloading. In

contrast, the stress of the 0.2 mm SMA wire phase change platform is higher than that of the other two wire diameters. Therefore, the energy density and energy conversion efficiency are higher than those of the other two SMA wires. Therefore, increasing the stress of the phase change platform during loading and unloading and reducing the stress difference between the platforms can improve energy conversion efficiency and significantly reduce energy loss.

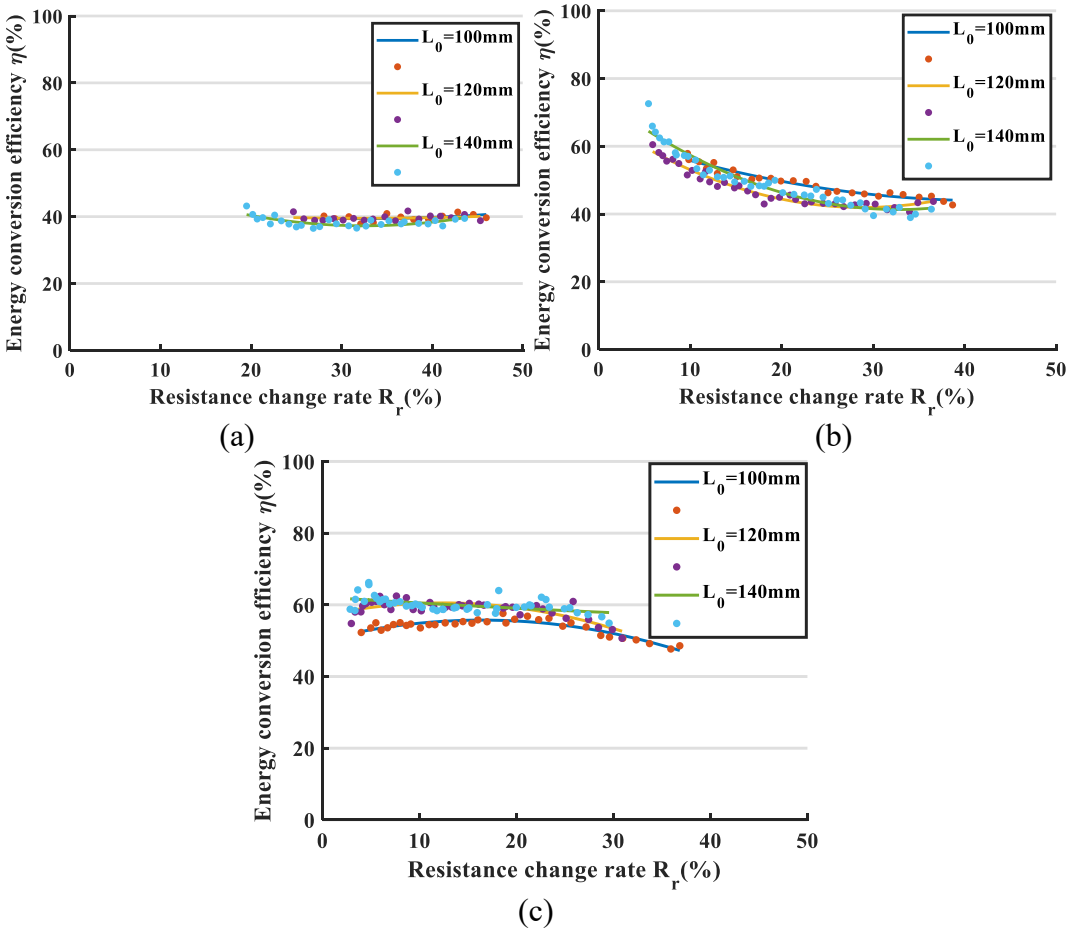


Fig. 13. Comparison of energy conversion efficiency under different wire diameters and lengths. (a) d = 0.1 mm. (b) d = 0.15 mm. (c) d = 0.2 mm.

4.4 Contrast with Steel Wire

In this section, steel wires of 0.1 mm and 0.2 mm are used for the comparison test.

Fig. 14 shows the comparison of the ejection energy density of steel wire and alloy wire under different strains. Fig. 15 is a comparison of the energy conversion efficiency with different wire diameters and different lengths between SMA wire and steel wire. Fig. 16 shows the comparison of the maximum velocity of the projectile during the test of steel wire and alloy wire, L_0 = 140 mm, d = 0.2 mm. Some oscillating waves after the maximum velocity are caused by the projectile falling on the wire again.

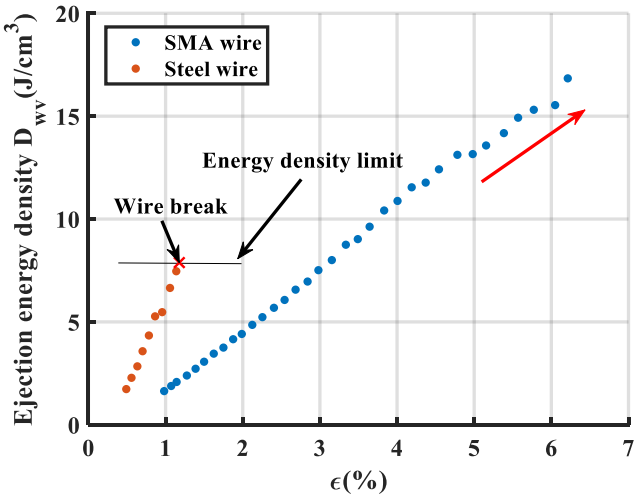


Fig. 14. Comparison of the ejection energy density of steel wire and SMA wire, L_0 = 100 mm, d = 0.2 mm.

As shown in Fig. 14, the maximum strain and maximum ejection energy density of the superelastic SMA wire are found to be at least one times higher than those of the steel wire. The ejection energy density of both the steel wire and SMA wire increases linearly with increasing strain. The steel wire breaks when the strain reaches approximately 1.2%, and the amount of energy storage is limited. SMA wire has superelasticity, the strain can exceed 6%, and the energy density far exceeds that of steel wire. According to Fig. 15, a comparison of the energy conversion efficiency of steel wires with different wire diameters and lengths confirms that the steel wires

have a high energy conversion efficiency rate of 72±15%. In the maximum ejection velocity of wire ejection tests, referring to Fig. 16, superelastic SMA wire has a higher velocity. In the steel wire ejection test, the maximum ejection velocity of the projectile is approximately 3 m/s. To ensure that the SMA wire does not break in the experiment, the strain is controlled within 7%, as defined in section 2. In the superelastic SMA wire ejection test, when the strain is over 6%, the maximum ejection velocity of the projectile can reach 4 m/s.

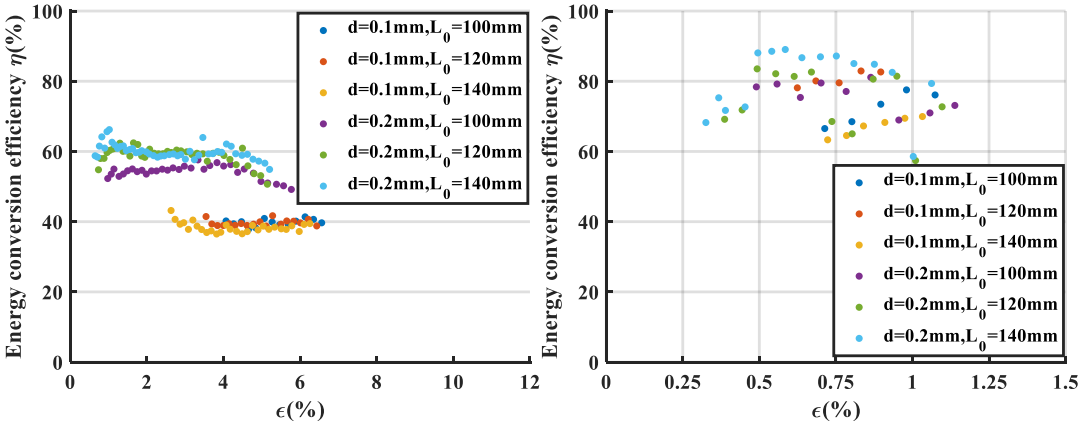


Fig. 15. Comparison of energy conversion efficiency. (a) SMA wire. (b) Steel wire.

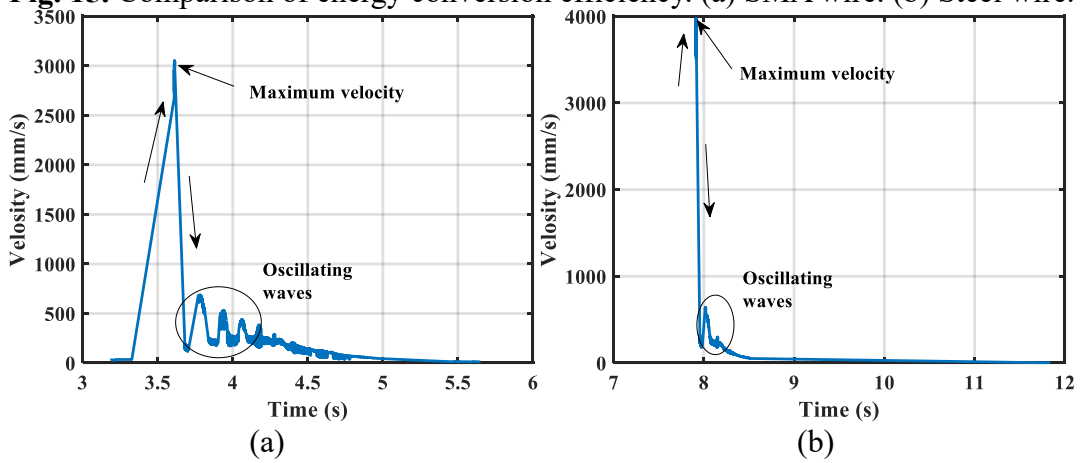


Fig. 16. Maximum ejection velocity. (a) Steel wire ejection test, d = 0.2 mm, L_0 = 140 mm. (b) SMA wire ejection test, d = 0.2 mm, L_0 = 140 mm.

In conclusion, superelastic SMA wires have excellent energy storage ejection characteristics when compared to steel wires. When the wire diameter and length are the same, the superelastic SMA wire can release at least twice the ejection energy as

the steel wire. SMA wire is superelastic and has a large recovery strain, whereas the steel wire is prone to plastic deformation and has no self-sensing characteristics.

5. Theoretical model establishment

According to the experimental results, a theoretical model is determined and established to to investigate and analyse the relationship between strain, resistance, and ejection energy density. This allows us to quantitatively predict the energy release and understand the self-sensing mechanism of SMA.

First, based on the linear relationship between the resistance change rate R_r and the strain ε observed in Fig. 11, R_r is defined as

$$R_{\mathrm{r}} = \kappa_R \varepsilon \tag{13}$$

where κ_R is the resistance strain constant of the superelastic SMA wire, which can be calculated based on the data obtained from the pretension test before ejection.

Before the energy storage ejection test, a large strain rapid tensile release test was performed on SMA wires of different wire diameters to obtain the stress–strain relationship. Then, a simple model is built based on the stress–strain relationship, as shown in Fig. 17. The theoretical model of the stress–strain relationship needs to be simplified according to the following criteria: In the simplified model of the hysteresis curve of the superelastic SMA wire, the elastic deformation stage of the austenite is consistent with the curve during the test, and the stress at which the transformation begins should be close to the transformation stress at the time of testing; considering

the existence of other energy losses during the test, the martensitic transformation stage can be slightly lower than the measured curve of the test; the martensite elastic deformation stage and the martensite reverse transformation stage should be as tangent as possible to the test curve during unloading.

According to the above criteria, the coordinate parameters in the experiment are selected and shown in Table 3. In this experiment, the maximum strain rate of SMA wire ejection can reach 700 s^{-1}, which is 70 times higher than the strain rate of 10^{-1} s^{-1} in E. Pieczyska's experimental study [19]. According to Fig. 11 and Fig. 12, the relationship between the ejection energy density and the resistance change rate of SMA wires with different wire diameters is not entirely consistent. Additionally, even the same batch of SMA wires will be different. The tests for theoretical model validation used a new batch of SMA wire, so the test results were marginally different from the test results in Section 2.

Table 3. The coordinate point parameters of the theoretical model.

Coordinate point	Stress & Strain	Wire diameter		
		0.1 mm	0.15 mm	0.2 mm
B	ε	0.001893	0.00078	0.0039
	σ	123.42 MPa	78.5 MPa	210 MPa
C	ε	0.006	0.00488	0.00762
	σ	458 MPa	310 MPa	446 MPa
E	ε	0.06	0.0614	0.06
	σ	560 MPa	597.5 MPa	638 MPa
F	ε	0.0475	0.0467	0.049
	σ	215 MPa	179 MPa	344 MPa

The resistance change rates κ_R of the 0.1 mm, 0.15 mm and 0.2 mm SMA wires were 6.967, 5.833 and 5.833, respectively.

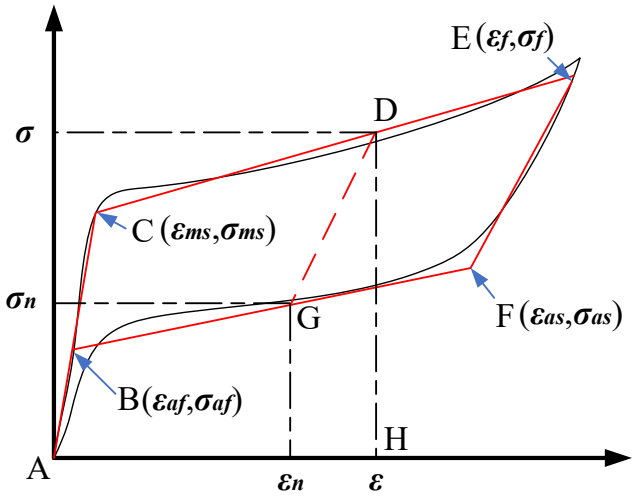


Fig. 17. Theoretical model based on SMA stress–strain relationship.

Fig. 17 shows the ejection energy density of the SMA wire when the strain ε is the area enclosed by the ABGDH.

The slope of the straight-line CE is $\kappa_{CE} = (\sigma_f - \sigma_{ms})/(\varepsilon_f - \varepsilon_{ms})$, the slope of the straight-line BF is $\kappa_{BF} = (\sigma_{as} - \sigma_{af})/(\varepsilon_{as} - \varepsilon_{af})$, the straight-line DG is parallel to the straight-line EF, and its slope is $\kappa_{DG} = (\sigma_f - \sigma_{as})/(\varepsilon_f - \varepsilon_{as})$. According to the geometric relationship, the following relationship can be obtained:

$$\sigma = \kappa_{CE}(\varepsilon - \varepsilon_{ms}) + \sigma_{ms} \tag{14}$$

$$\sigma = \kappa_{BF}(\varepsilon - \varepsilon_{af}) + \sigma_{af} \tag{15}$$

$$\sigma_n = \kappa_{DG}(\varepsilon_n - \varepsilon) + \sigma \tag{16}$$

It can be obtained by equations (13)-(16)

$$\sigma(R_r) = \kappa_{CE}\left(\frac{1}{\kappa_R} R_r - \varepsilon_{ms}\right) + \sigma_{ms} \tag{17}$$

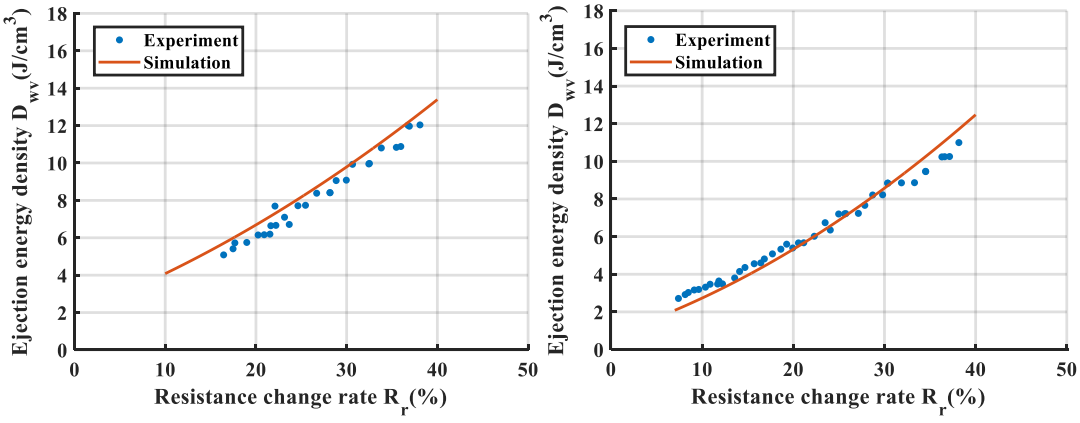
$$\varepsilon_n(R_r)=\frac{\varepsilon_{af}-\frac{\kappa_{DG}}{\kappa_{BF}\kappa_R}R_r+\frac{\sigma(R_r)}{\kappa_{BF}}}{1-\frac{\kappa_{DG}}{\kappa_{BF}}} \tag{18}$$

$$\sigma_n(R_r)=\kappa_{DG}(\varepsilon_n(R_r)-\frac{1}{\kappa_R}R_r)+\sigma(R_r) \tag{19}$$

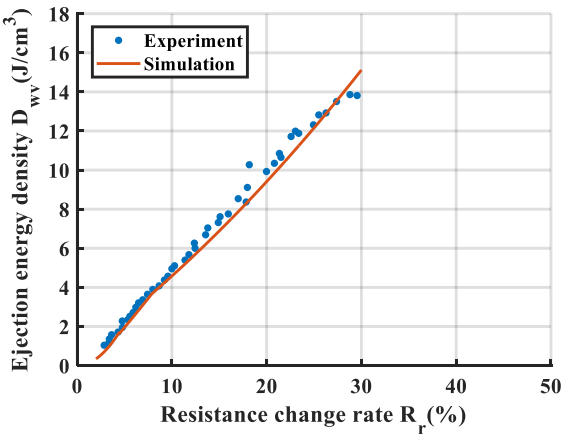
From equations (13)-(19), the relationship between the ejection energy density and resistance change rate can be obtained

$$D_{WV}(R_r)=\begin{cases}\dfrac{\sigma_{ms}}{2\varepsilon_{ms}\kappa_R^2}(R_r)^2 & (\varepsilon<\varepsilon_{ms})\\ \dfrac{\sigma_{af}R_r}{2\kappa_R}+\dfrac{1}{2}\sigma(R_r)(\dfrac{1}{\kappa_R}R_r-\varepsilon_{af}) & (\varepsilon>\varepsilon_{ms},\varepsilon_n<\varepsilon_{af})\\ \dfrac{\sigma_{af}\varepsilon_n(R_r)+\sigma_n(R_r)(\frac{1}{\kappa_R}R_r-\varepsilon_{af})+\sigma(R_r)(\frac{1}{\kappa_R}R_r-\varepsilon_n(R_r))}{2} & (\varepsilon_n>\varepsilon_{af})\end{cases} \tag{20}$$

The established theoretical model and the experimental results are shown for comparison in Fig. 18. Fig. 18 (a-c) suggest that the theoretical model is applicable to SMA wires of different wire diameters. Additionally, by measuring the resistance, the ejection energy density can be predicted, and then the energy released by the SMA wire can be predicted.



(a) (b)



(c)

Fig. 18. Comparison of ejection energy density between theory and experiment. (a) d = 0.1 mm, L_0 = 140 mm. (b) d = 0.15 mm, L_0 = 140 mm. (c) d = 0.2 mm, L_0 = 140 mm.

6. Conclusions

For the first time, this paper confirms that the energy of superelastic SMA wires can be quantatively measured by electrical resistence. This revolutionary characteristic in superelastic SMA materials will enable novel applcations, espcally in the energy ejection fileds.

In the wire ejection test, the superelastic SMA wire can release energy at least two times as high as the steel wire, and it has a linear relationship between the resistance change rate and strain. A theoretical prediction model of ejection energy density is developed based on the stress–strain diagram obtained from the multiple tensile tests. This theoretical model reveals the same findings as the in-house test on the relationship between ejection energy density and resistance change rate.

The limitation in the wire test is that the energy conversion efficiency of the superelastic SMA wire is approximately 10% lower than that of steel. The mechanical energy storage loss is mainly affected by the material processing technology and

atomic ratio. In future work, some material processing methods, such as decreasing the difference between the loading and unloading phase transition stress, need to be further studied to increase the energy storage efficiency of SMA wires.

In conclusion, the superelastic SMA is an advanced material with self-sensing and measurable energy storage ejection characteristics. This material has inherent advantages in designing ejection take-off devices. This paper designed and deployed state-of-the-art experiments in testing the relationship between resistance and energy in laboratory tests and theoretical models. This finding lays a foundation for designing next-generation energy storage ejection devices, such as unmanned aircraft, ejection seats on aircraft, and long-distance throwing cable devices. The superelastic SMA wire has high potential application value in broader energy storage ejection fields and engineering devices, particularly medical devices.

CRedit authorship contribution statement

Wen-Chao Sui: Conceptualization, Methodology, Investigation, Formal analysis, Validation, Data curation, Writing - original draft. **Yong-Chen Pei:** Conceptualization, Methodology, Formal analysis, Writing - review & editing, Validation, Supervision, Funding acquisition. **Hui-Qi Lu:** Validation, Methodology, Supervision, Writing - review & editing. **Bao-Hua Wang:** Validation, Writing - review & editing. **Ji-Tuo Wu:** Writing - review & editing.

Declaration of Competing Interest

The authors declare that they have no known competing financial interests or personal relationships that could have appeared to influence the work reported in this paper.

References

[1] M.H. Elahinia, M. Hashem, M. Tabesh, S.B. Bhaduri, Manufacturing and processing of NiTi implants: A review, Progress in Materials Science, 57 (2012) 911-946. https://doi.org/10.1016/j.pmatsci.2011.11.001.

[2] J.M. Jani, M. Leary, A. Subic, M.A. Gibson, A review of shape memory alloy research, applications and opportunities, Materials & Design, 56 (2014) 1078-1113. https://doi.org/10.1016/j.matdes.2013.11.084.

[3] S. Josephine, K. Dhanalakshmi, Shape memory alloy wire for self-sensing servo actuation, Mechanical Systems and Signal Processing, 83 (2017) 36-52. https://doi.org/10.1016/j.ymssp.2016.05.042.

[4] J.H. Guan, Y.C. Pei, J.T. Wu, A driving strategy of shape memory alloy wires with electric resistance modeled by logistic function for power consumption reduction, Mechanical Systems and Signal Processing, 160 (2021) 107839. https://doi.org/10.1016/j.ymssp.2021.107839.

[5] J. Li, Position control based on the estimated bending force in a soft robot with tunable stiffness, Mechanical Systems and Signal Processing, 134 (2019) 106335.106331-106335.106317. https://doi.org/10.1016/j.ymssp.2019.106335.

[6] J.E. Bidaux, R. Gotthardt, Elastic Behavior: Superelasticity, Encyclopedia of Materials Science & Technology, (2016). https://doi.org/10.1016/B978-0-12-803581-8.02942-8.

[7] C. Lan, C.H. Fan, Investigation on pretensioned shape memory alloy actuators for force and displacement self-sensing, 2010 IEEE/RSJ International Conference on Intelligent Robots and Systems, October 18-22, 2010, Taipei, Taiwan, 2010.

[8] W.M. Huang, Z. Ding, C.C. Wang, J. Wei, Y. Zhao, H. Purnawali, Shape memory materials, Materials Today, 13 (2010) 54-61. https://doi.org/10.1016/S1369-7021(10)70128-0.

[9] S. Zareie, A.S. Issa, A. Zabihollah, R.J. Seethaler, Recent Advances in the Applications of Shape Memory Alloys in Civil Infrastructures: A Review, Structures, 27 (2020). https://doi.org/10.1016/j.istruc.2020.05.058.

[10] C.S. Wen, X.J. Yu, W. Zeng, S. Zhao, L. Wang, G.C. Wan, S.C. Huang, H.

Grover, Z. Chen, Mechanical behaviors and biomedical applications of shape memory materials: A review, AIMS Mater. Sci., 5 (2018) 559-590. https://doi.org/10.3934/matersci.2018.4.559.

[11] G. Costanza, M.E. Tata, Shape Memory Alloys for Aerospace, Recent Developments, and New Applications: A Short Review, Materials, 13 (2020). https://doi.org/10.3390/ma13081856.

[12] S. Barbarino, E.S. Flores, R.M. Ajaj, I. Dayyani, M.I. Friswell, A review on shape memory alloys with applications to morphing aircraft, Smart Materials and Structures, 23 (2014) 063001. https://doi.org/10.1088/0964-1726/23/6/063001.

[13] C. Naresh, P.S.C. Bose, C.S.P. Rao, Shape memory alloys: a state of art review, Iop Conference, 149 (2016) 012054. https://doi.org/10.1088/1757-899X/149/1/012054.

[14] S. Hao, L. Cui, D. Jiang, C. Yu, Nanostructured Nb reinforced NiTi shape memory alloy composite with high strength and narrow hysteresis, Applied Physics Letters, 102 (2013) 511. https://doi.org/10.1063/1.4809954.

[15] A. Alipour, M. Kadkhodaei, M. Safaei, Design, analysis, and manufacture of a tension–compression self-centering damper based on energy dissipation of pre-stretched superelastic shape memory alloy wires, Journal of Intelligent Material Systems & Structures, 28 (2017) 1045389X1668283. https://doi.org/10.1177/1045389X16682839.

[16] S.C. Kwon, H.U. Oh, Passive micro-jitter isolation of gimbal-type antenna by using a superelastic SMA gear wheel, Mechanical Systems and Signal Processing, 114 (2018) 35-53. https://doi.org/10.1016/j.ymssp.2018.05.001.

[17] S.B. Kumbhar, S.P. Chavan, S.S. Gawade, Adaptive tuned vibration absorber based on magnetorheological elastomer-shape memory alloy composite, Mechanical Systems and Signal Processing, 100 (2018) 208-223. https://doi.org/10.1016/j.ymssp.2017.07.027.

[18] I. Schmidt, R. Lammering, The damping behaviour of superelastic NiTi components, Materials Science & Engineering A, 378 (2004) 70-75. https://doi.org/10.1016/j.msea.2003.09.106.

[19] E. Pieczyska, W. Nowacki, T. Sakuragi, H. Tobushi, Superelastic Deformation Properties of TiNi Shape Memory Alloy, Key Engineering Materials, 340 (2007) 1211-1216. https://doi.org/10.4028/www.scientific.net/KEM.340-341.1211.

[20] Z.Q. Liu, H. Li, W.L. Chen, J.P. Ou, Study on Strain-sense Property of TiNi and TiNiCu Shape Memory Alloys, Advances in Structural Engineering, 8 (2005) 637-643. https://doi.org/10.1260/136943305776318374.

[21] K. Fushimi, L. Neelakantan, G. Eggeler, A.W. Hassel, On the Electropolishing Mechanism of Nickel Titanium in Methanolic Sulfuric acid An Electrochemical Impedance Study, physica status solidi (a), 215 (2018) 1800011.1800011-1800011.1800016. https://doi.org/10.1002/pssa.201800011.

[22] O. Rubes, J. Chalupa, F. Ksica, Z. Hadas, Development and experimental

validation of self-powered wireless vibration sensor node using vibration energy harvester, Mechanical Systems and Signal Processing, 160 (2021) 107890. https://doi.org/10.1016/j.ymssp.2021.107890.

[23] Z.G. Wei, R. Sandstrorm, S. Miyazaki, Shape-memory materials and hybrid composites for smart systems: Part I Shape-memory materials, Journal of Materials Science, 33 (1998) 3743-3762. https://doi.org/10.1023/A:1004674630156.

[24] V. Apostol, N.M. Lohan, E. Mihalache, R.I. Comăneci, N. Cimpoesu, B. Pricop, M. Popa, L.G. Bujoreanu, Accumulation of stress induced martensite in Fe43.5Mn34Al15±xNi7.5∓X shape memory alloys, IOP Conference Series: Materials Science and Engineering, 572 (2019) 012032. https://doi.org/10.1088/1757-899X/572/1/012032.

[25] E.M. Sharifi, A. Kermanpur, Superelastic behavior of nanostructured Ti 50 Ni 48 Co 2 shape memory alloy with cold rolling processing, Transactions of Nonferrous Metals Society of China, 28 (2018) 1351-1359. https://doi.org/10.1016/S1003-6326(18)64773-9.